

RESEARCH

Open Access



Integrative analysis of T cell-mediated tumor killing-related genes reveals KIF11 as a novel therapeutic target in esophageal squamous cell carcinoma

Xinxin Cheng^{1†}, Huihui Zhao^{4†}, Zhangwang Li¹, Liping Yan⁵, Qingjie Min¹, Qingnan Wu^{1,2*} and Qimin Zhan^{1,2,3*} 

Abstract

Background Immune checkpoint inhibitors (ICIs) are emerging promising agents for the treatment of patients with esophageal squamous cell carcinoma (ESCC), however, there are only a small proportion respond to ICI therapy. Therefore, selecting candidate patients who will benefit the most from these drugs is critical. However, validated biomarkers for predicting immunotherapy response and overall survival are lacking. As the fundamental principle of ICI therapy is T cell-mediated tumor killing (TTK), we aimed to develop a unique TTK-related gene prognostic index (TTKPI) for predicting survival outcomes and responses to immune-based therapy in ESCC patients.

Methods Transcriptomic and clinical information of ESCC patients were from the GSE53625, GSE53624, GSE47404 and TCGA datasets. TTK-related genes were from the TISIDB database. The LASSO Cox regression model was employed to create the TTKPI. The prediction potential of the TTKPI was evaluated using the KM curve and time-dependent ROC curve analysis. Finally, the relationship between TTKPI and immunotherapy efficacy was investigated in clinical trials of ICIs (GSE91061, GSE135222, IMvigor210 cohort). The role of KIF11 in accelerating tumor progression was validated via a variety of functional experiments, including western blot, CCK-8, colony formation, wound healing scratch, and xenograft tumor model. The KIF11 expression was detected by multiplex fluorescent immunohistochemistry on tissue microarray from ESCC patients.

Results We constructed the TTKPI based on 8 TTK-related genes. The TTKPI low-risk patients exhibited better overall survival. TTKPI was significantly and positively correlated with the main immune checkpoint molecules levels. Furthermore, the low-risk patients were more prone to reap the benefits of immunotherapy in the cohort undergoing anti-PD-L1 therapy. Moreover, we performed functional experiments on KIF11, which ranked as the most significant prognostic risk gene among the 8 TTK-related genes. Our findings identified that KIF11 knockdown significantly hindered cell proliferation and mobility in ESCC cells. The KIF11 expression was negatively related with CD8⁺ T cell infiltration in ESCC patient samples.

[†]Xinxin Cheng and Huihui Zhao authors contributed equally to this work.

*Correspondence:

Qingnan Wu
wuqingnan@bjmu.edu.cn
Qimin Zhan
zhanqimin@bjmu.edu.cn

Full list of author information is available at the end of the article



Conclusions The TTKPI is a promising biomarker for accurately determining survival and predicting the effectiveness of immunotherapy in ESCC patients. This risk indicator can help patients receive timely and precise early intervention, thereby advancing personalized medicine and facilitating precise immuno-oncology research. KIF11 plays a crucial role in driving tumor proliferation and migration and may act as a potential tumor biomarker of ESCC.

Keywords ESCC, T cell-mediated tumor killing, Immunotherapy, Prognostic signature, KIF11

Background

Esophageal cancer is one of the most prevalent digestive malignancies and the 6th most common cause of cancer death worldwide [1]. China accounts for over 70% of all global cases, with esophageal squamous cell carcinoma (ESCC) presenting as the most common type [1]. Owing to lacking effective early diagnosis and management techniques, the 5-year survival rate of ESCC patients is as low as 20% [2–4]. At present, immunotherapy has become a novel important treatment for ESCC [5].

Cancer immunotherapies utilizing immune checkpoint inhibitors (ICIs) assist the immune system in recognizing and attacking tumor cells [6, 7]. Programmed death protein 1 (PD-1), programmed death-ligand 1 (PD-L1), and cytotoxic T-lymphocyte-associated protein 4 (CTLA4) are primary targets of ICI therapy [8–10]. The clinical use of immunotherapies targeting immune checkpoints has recently significantly improved the clinical effects and changed the ESCC treatment paradigm [11, 12]. Nonetheless, the clinical prognosis tends to be unfavorable due to a high incidence of recurrence, metastasis, and drug resistance [13–17].

Several biomarkers, including PD-L1 expression and tumor mutation features, are frequently employed in clinical settings to predict immunotherapy response [18–20]. However, only a minority of patients benefit from immunotherapy [19]. Some studies demonstrated that the immune-related status could serve as a primary prognostic indicator, further enhancing targeted therapy efficacy [21]. Several immune-related gene signatures have been developed to predict treatment outcomes in patients with ESCC [22]. However, the accuracy of predicting outcomes is often insufficient for clinical application. Therefore, a more comprehensive and reliable signature is urgently needed to accurately predict overall survival (OS) and immunotherapy efficacy of ESCC patients accurately.

Given the vital roles of T cells in immunity, earlier research has explored the molecular features of T cells in infectious diseases and cancers; however, a comprehensive molecular analysis of T cell-mediated tumor killing (TTK) in ESCC is devoid [23]. TTK-related genes have been identified using CRISPR screening and high-throughput experimental methods [23, 24]. Hence, developing a TTK-related gene signature that is closely

associated with the immune status is both appropriate and viable for predicting immunotherapy efficacy.

The kinesin superfamily (KIF), microtubule-based molecular motors, comprises 14 families (Kinesin 1–14A/B) mediating intracellular transport [25, 26]. KIF11, also known as Eg5, exerts vital cellular functions and is required for chromosome positioning and separation, mitotic spindle formation as well as maintenance, and mitosis drivers [27–29]. Recently, an emerging number of studies have proven that KIF11 is aberrantly upregulated in different cancers, accelerating tumor development and progression. KIF11 was demonstrated to drive glioblastoma invasion, proliferation, and self-renewal [30]. High KIF11 expression enhances the proliferation of gallbladder cancer cells through ERBB2-mediated activation of downstream signaling pathway [31]. Furthermore, inhibition of KIF11 can inhibit pancreatic ductal adenocarcinoma cell proliferation, promote apoptosis, and increase sensitivity to chemotherapy [32]. However, there is limited research discussing the correlation between KIF11 and ESCC.

In this study, we developed a prognostic index termed TTKPI (TTK-related gene prognostic index) and demonstrated its predictive potential as an indicator for evaluating the effectiveness of immunotherapy. The newly developed TTKPI could be a valuable tool for guiding cancer immunotherapy for patients with ESCC. In addition, KIF11 was ultimately identified as the most significant prognostic risk gene and was verified to promote the proliferation, invasion, and growth in ESCC. All results suggest that KIF11 has great potential as a valuable predictive biomarker and therapeutic target.

Methods

Data acquisition and preprocessing

TTK-related genes were curated from the TISIDB database and compiled to form a gene set referred to as TTKs [24], and details are shown in Supplementary Table 1. The data of ESCC samples was collected from the Gene Expression Omnibus (GEO) (<https://www.ncbi.nlm.nih.gov/geo>) and The Cancer Genome Atlas (TCGA) (<https://www.cancer.gov/tcga/>), including GSE53625 cohort (n = 179), GSE53624 (n = 119), GSE47404 (n = 68) and the TCGA-ESCC cohort (n = 83) [33, 34]. The GSE53625 was

served as the training set. The GSE53624, GSE47404 and TCGA cohort were served as the external validation sets. A detailed overview of the sample characteristics and clinical data for GSE53625 is presented in Supplementary Table 2.

Differentially expressed TTK-related genes

Differentially expressed genes (DEGs) in 179 ESCC precancerous and cancerous tissues were discovered utilizing the "limma" package [35] ($|\log_2FC| > 1$ and adjusted $P < 0.05$). To construct and visualize TTK-related DEGs, we intersected these DEGs with TTK-related genes to generate volcano plots by package "ggplot2" [36] and a Venn diagram via a webtool (<https://bioinformatics.psb.ugent.be/webtools/Venn/>).

Pathway and function enrichment analysis

Enrichment analysis for investigating the biological functions of TTK-related DEGs was conducted via the "clusterProfiler" package [37]. The functional enrichment of GO terms and the KEGG signaling pathways were determined using a 5% false discovery rate. Significant enrichment was defined based on $P < 0.05$.

TTK-related gene prognostic signature construction and validation

The impact of TTK-related DEGs on ESCC survival was examined by the Univariate Cox regression analysis with $P < 0.05$. Consequently, 10 TTK-related DEGs significantly affecting OS were identified. The candidates were further narrowed down, and an optimal signature was constructed using The LASSO Cox regression [38]. Specifically, we utilized the "lambda.min" value, determined by the "glmnet" package [39]. Following the analysis, the model ultimately generated and exported the TTKPI for each patient using the following formula:

$$\text{TTKPI} = \sum_{i=1}^8 (\beta_i \times E_i)$$

where β_i represents the risk coefficient; E_i represents the expression of each gene. A linear transformation was applied to the TTKPI to improve the intuitiveness of the plots. The package "MaxStat" was utilized to calculate the best threshold for separating ESCC patients into two groups (low- and high-risk) [40]; the ideal cutoff point was 0.61. The "stats" package was used to conduct principal component analysis. Furthermore, the R packages of "survival" and "survminer" were employed to conduct a Kaplan–Meier (KM) analysis to further explore the relationship between TTKPI and OS [41, 42].

Establishment of the prognostic nomogram

A prognostic nomogram was constructed by integrating clinical characteristics (sex, age, grade, stage, and alcohol consumption) with TTKPI using the "rms" and "regplot" packages in R, following the multivariable stepwise Cox regression analysis results [43]. Time-dependent receiver operating characteristic (ROC) curves were generated to assess the prognostic models. The "timeROC" package was employed to plot the ROC curve analysis, and the area under the curve (AUC) values were calculated to determine the predictive performance of each model. Additionally, calibration curves were generated by the "rms" package to assess the predictive performance of the nomogram and compare predicted survival with actual survival.

Analysis of immunotherapy efficacy

GSE91061, GSE135222, IMvigor210 were used to confirm the feasibility and reliability of the TTKPI to predict the ICI therapy response [44–47]. Patients were classified into two categories—responders and non-responders—for comparison based on treatment outcomes. Responders reached complete response, very good partial response or stable disease, while non-responders experienced progressive disease.

Cell lines and cell culture

The human ESCC cell lines YES2, KYSE30, KYSE150, KYSE410, KYSE450, and KYSE510 were authenticated by short tandem repeat analysis. Cells were maintained in RPMI-1640 medium (Lonza, Switzerland) with 10% fetal bovine serum (Gibco, USA) and 1% penicillin/streptomycin (Gibco, USA), under standard conditions in a humidified incubator at 37 °C and 5% CO₂.

Lentivirus infections

For KIF11 knockdown, lentivirus encoding specific short hairpin RNA (shRNA) was developed by Shanghai Jikai Gene Chemical Technology. After lentiviral infection, stable clones were selected by treatment of the cells with puromycin (2 µg/mL, Sigma-Aldrich, USA). The shRNA information are listed as follows: sh1: 5'- TACAGCAGA AATCTAAGGATA -3'; sh2: 5'- CGTAACAAGAGA GGAGTGATA -3'; NC: 5'- TTCTCCGAACGTGTC ACGT -3'.

Western blotting

All cells used in our study were lysed using 1% NP-40 lysis buffer containing protease inhibitor cocktail (Roche, Mannheim, Germany). Extracted protein samples were then separated through SDS-PAGE and electrophoretically transferred to PVDF membranes, which were blocked in 5% bovine serum albumin (BSA) and

incubated overnight at 4 °C with the primary antibodies. This was followed by 1-h incubation with secondary antibodies at room temperature. Signals were detected with chemiluminescence and imaged using the Amersham Imager 600 (GE Healthcare, USA). Following antibodies were used for Western blotting: KIF11 (A7907, Abclonal, China) and β -actin (Ab8226, Abcam, USA).

Colony-formation assay

ESCC cells were seeded in 6-well plates at a density of 1×10^3 cells per well. After 10 days, cells were washed with cold PBS (3 times), fixed with ice-cold methanol (10 min), and stained with 0.1% crystal violet (10 min). The cultures were then rinsed with deionized water and imaged under a microscope.

CCK-8 assay

Cell viability was evaluated by the CCK-8 assay kit (K1018, Apexbio, USA). 1×10^4 cells/well were plated in a 96-well plate. At indicated time intervals (0, 24, 48, and 72 h), 10 μ L CCK-8 solution was then added to each well, followed by 2 h incubation at 37 °C. Then, absorbance was measured at 450 nm by a microplate reader (Bio-Rad, Hercules, CA, USA).

Wound-healing scratch assay

Cells were grown on 6-well plates until confluence and then scratched using a 200- μ L pipette tip to create a straight "wound" path. Next, PBS was applied to remove the dislodged cells. Subsequently, the cells were incubated with culture medium with 2% FBS for 20 h. All wounds were captured and measured at the start (0 h) and 20 h post-wounding.

Xenograft tumor model

Female BALB/c nude mice were purchased from Beijing Vital River Laboratories (aged 5 weeks, China). Cell suspensions containing 5×10^6 stable transfected KYSE30 cells in 100 μ L PBS premixed with Matrigel gel were subcutaneously injected into the right lower flanks of the nude mice ($n=8$ mice/group). Tumor measurements began 7 days after injection and were recorded every 2 days to track growth. Xenograft tumors were harvested and measured after 24 days. Tumor volumes were calculated by a standard formula: $\text{volume} = 1/2 \times \text{length} \times \text{width}^2$. All experiments were conducted following the approval from the Institutional Animal Care and Use Committee of Peking University Cancer Hospital and Institute.

Multiplex fluorescent immunohistochemistry (mIHC)

Tissue microarray slides from ESCC patients were purchased from Zhongke Guanghai Biotech Co., Ltd (Xi'an,

China). mIHC staining of KIF11 (Abclonal, Cat#: A7907), CD8 (Abcam, Cat#: ab101500), and S100 (Abcam, Cat#: ab52642) was performed using TG TSA Multiplex IHC Assay Kits (TissueGnostics Asia-Pacific Ltd.). The visualization of various fluorophores was conducted using the TissueFAXS Spectra System (TissueGnostics GmbH, Vienna, Austria) along with StrataQuest analysis software (Version 7.1.129, TissueGnostics GmbH, Vienna, Austria).

Statistical analysis

All data was analysed with R (version 4.0.2) and GraphPad Prism (version 8.0). Student's t-test and Wilcoxon test were applied to compare two independent groups. KM survival plots were generated to visualize survival curves and comparisons were made using the Log-rank statistical analysis. $P < 0.05$ was assumed to indicate statistical significance.

Results

Identification of TTK-related DEGs

The study flowchart was shown in Fig. 1a. In the GSE53625 cohort, we identified 2,322 DEGs (adjusted $P < 0.05$ and $|\log_2 \text{FC}| > 1$) between tumor and healthy samples. Overall, 924 genes were upregulated, whereas 1,398 genes were downregulated in ESCC group compared to the healthy group (Fig. 1b, Supplementary Figs. 1a, b). After intersecting 1,109 TTK-related genes with 2,322 DEGs, 98 TTK-related DEGs were identified for further analysis (Fig. 1c). Among these 98 DEGs, 56 genes were upregulated and 42 were downregulated in the tumor samples (Fig. 1d). The landscape of TTK-related DEGs between healthy and tumor tissues was clearly shown by hierarchical clustering (Fig. 1e). Furthermore, the GO analysis on these 98 genes revealed that the most enriched term was "mitotic sister chromatid segregation" (Fig. 1f). We also investigated the genes associated with the top terms, the functions of which require further exploration (Supplementary Fig. 1c). Moreover, the KEGG analysis indicated that the upregulated gene set was primarily associated with "measles" and the "transforming growth factor-beta signaling pathway", while the downregulated gene set was mostly associated with "biosynthesis of nucleotides sugars" (Fig. 1g). In summary, the identification and analysis of 98 TTK-related DEGs revealed significant gene expression differences between tumor and healthy tissues, with enriched pathways providing potential insights into ESCC development and progression.

TTK-related prognostic signature construction

To create a biomarker for predicting the prognosis of ESCC patients based on TTK-related DEGs, a risk score

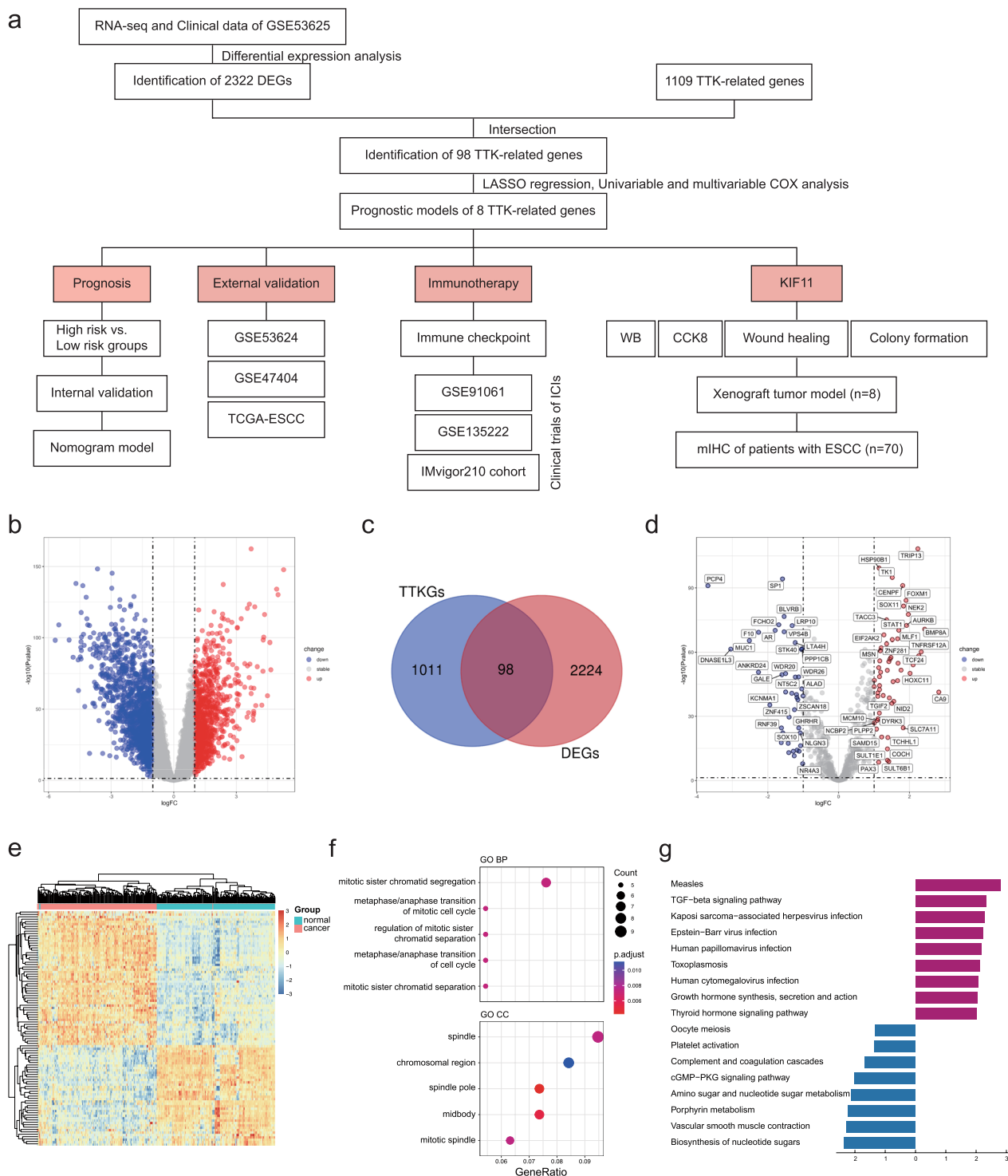


Fig. 1 Investigation of TTK-related DEGs. **a** The flowchart of this study. **b** Volcano plot shows 2322 of 15,145 genes that were differentially expressed in patients with ESCC from the GSE53625 cohort (blue: down-regulated; red: up-regulated; grey: unchanged). **c** Venn diagram visualizing the intersections between DEGs and TTK-related genes. **d** Volcano plot of 98 TTK-related DEGs. **e** The expression heatmap of all 98 TTK-related DEGs is displayed. (Blue: down-regulated; red: up-regulated; each row representing differentially expressed genes; each column representing samples). **f** GO analysis of 98 TTK-related DEGs. **g** The top upregulated and downregulated pathways derived from KEGG analysis of 98 TTK-related DEGs is shown

prediction model was developed. Initially, univariate Cox regression analysis was applied to identify genes significantly associated with survival outcomes. In the GSE53625 cohort, 10 TTK-related DEGs met the significance threshold of $P < 0.05$. Subsequently, LASSO regression analysis and cross-validation were performed, yielding LASSO regression curves and cross-validation plots (Figs. 2a, b). Finally, an 8-gene signature (KIF11, SLC2A1, KCNMA1, BARHL2, CA9, TIMP1, MAGEC3, and PDZK1IP1) was constructed using the following LASSO cox regression approach:

$$\text{TTKPI: } (0.0552283605 \times \text{KIF11 exp.}) + (-0.0070408017 \times \text{SLC2A1 exp.}) + (0.0194419232 \times \text{KCNMA1 exp.}) + (-0.0231625843 \times \text{BARHL2 exp.}) + (-0.0214342225 \times \text{CA9 exp.}) + (0.0161917634 \times \text{TIMP1 exp.}) + (-0.0712586182 \times \text{MAGEC3 exp.}) + (-0.0004431282 \times \text{PDZK1IP1 exp.}).$$

Furthermore, the prognostic significance of 8 TTK genes was evaluated through univariate Cox regression analysis, identifying KIF11 as the most significant prognostic factor. Forest plots were used to visually illustrate the relationship between each of the 8 genes and

the prognosis of ESCC patients (Fig. 2c). Additionally, using the optimal cutoff point of TTKPI calculated from the above formula, 179 ESCC patients in the GSE53625 cohort were stratified into two distinct risk groups: low-risk and high-risk (Fig. 2d). To assess the stability of key molecule expression, we examined the 8 specific genes expression in the two groups (Fig. 2e). Taken together, an 8-gene TTK-related signature was established as a risk score prediction model, effectively stratifying ESCC patients into low-risk and high-risk groups and demonstrating its potential as a reliable prognostic biomarker.

Train and validate the risk score model for ESCC patients

We analyzed the OS of ESCC patients with different TTKPI levels. High TTKPI levels correlated with shorter survival times ($P < 0.05$; Fig. 3a, b). The ROC curve in the GSE53625 cohort also indicated that the developed TTKPI had a high potential to monitor the OS of ESCC patients (Fig. 3c, the AUC at 1-year: 0.69, 3-year: 0.67, and 5-year: 0.70). In addition, we performed validation in three external datasets separately, including

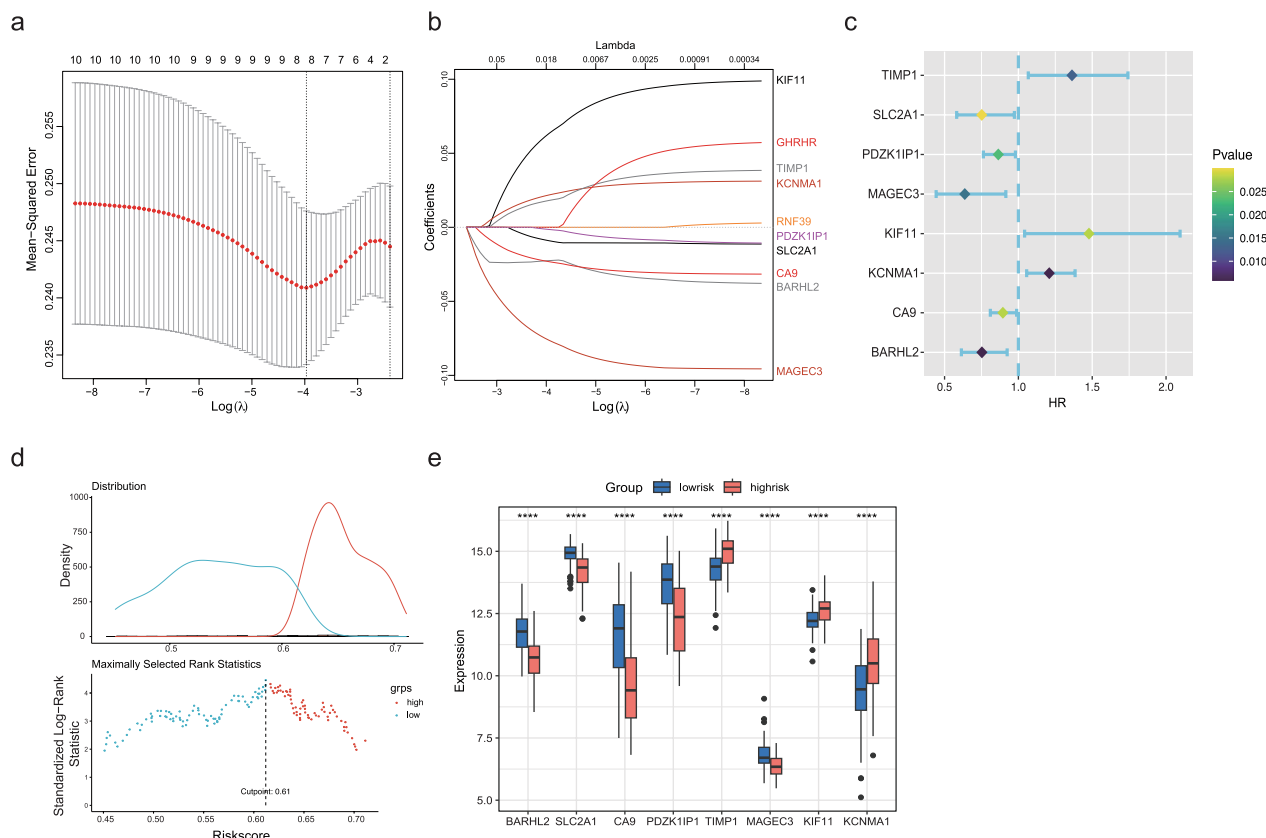


Fig. 2 Construction and validation of an immune-related gene signature prediction model. **a** LASSO regression analysis to identify signature genes. **b** Cross-validation of the constructed signature. **c** Forest plot presenting the univariate cox regression analysis results of each TTKPI-related gene. **d** Distribution of risk scores and **(e)** Expression levels of 8 selected genes between the high-risk and low-risk ESCC patients. Statistical analysis is performed with Log-rank test **(c)** and Student's t-test **(e)**. **** $P < 0.0001$

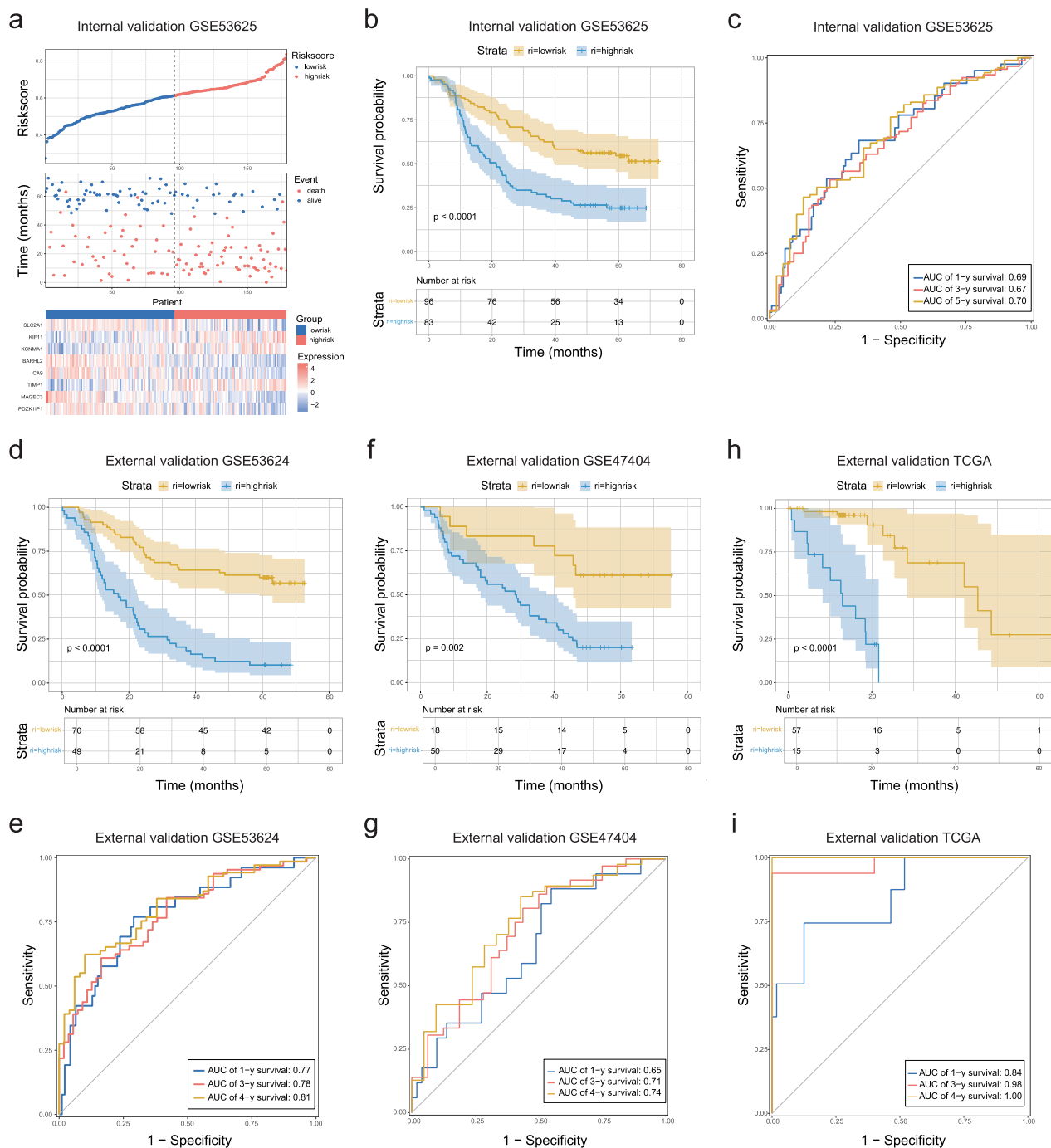


Fig. 3 Training and validation of the gene signature prognostic mode. **a** Risk score distribution, and expression of the 8 model genes for ESCC patients in the low-risk and high-risk groups **b** KM survival analysis and **c** ROC analysis of the survival rates of patients in the GSE53625 cohort (n = 179) (Internally validated). **d, f, h** Externally validated KM survival analysis for the high-risk and low-risk groups in the GSE53624 cohort (**d**), GSE47404 cohort (**f**) and TCGA-ESCC cohort (**h**). **e, g, i** Externally validated ROC analysis for the high-risk and low-risk groups in GSE53624 cohort (**e**), GSE47404 cohort (**g**) and TCGA-ESCC cohort (**i**). Statistical analysis is performed with Fisher's exact test (**f, h, i**) and Log-rank test (**d, g, i**). AUC: area under the curve; ROC: receiver operating characteristic

GSE53624 (n=119), GSE47404 (n=68) and the TCGA-ESCC cohort (n=83). KM curve indicated that high-risk patients had shorter OS and a worse prognosis ($P < 0.05$, Fig. 3d, f, h). Furthermore, the AUC values for 1-, 3-, and 4-year survival rates in the three external validation sets respectively demonstrated that TTKPI has good prognostic predictive capability (Fig. 3e, g, i). This result indicated that the TTKPI had a high accuracy in predicting the survival of ESCC patients.

Establish and assess the nomogram model forecasting survival

To assess the predictive value of TTKPI, both univariate and multivariate analyses were employed using Cox regression analysis. (Fig. 4a and Supplementary Fig. 1d). The TTKPI was observed as an independent prognostic factor after adjusting for other clinicopathological factors (HR: 60.51, 95% confidence interval [CI]: 8.869–412.907, $P < 0.001$) in patients with ESCC. Moreover, we developed a predictive nomogram using multivariable Cox and stepwise regression analyses based on the TTKPI and several clinicopathological characteristics to offer a quantitative analytical tool to forecast individual patients' OS rates. The model included age, sex, grade, stage, alcohol consumption, and the TTKPI (Fig. 4b). The model prediction accuracy of the 1-, 3-, and 5-year survival probabilities was validated with calibration curves, further supporting its clinical utility in forecasting patient outcomes (Fig. 4c). In summary, these analyses demonstrate that TTKPI serves as a robust independent prognostic factor for ESCC patients. The development of a predictive nomogram incorporating TTKPI alongside key clinicopathological characteristics offers a valuable tool for personalized survival predictions.

TTKPI predicts the clinical response to immunotherapy

Improving immunotherapeutic efficacy via immune checkpoint inhibition significantly advances cancer treatment. Therefore, we explored the immune checkpoint expressions of the two groups and found that the risk score value was positively correlated with the levels of the main immune checkpoint molecules (PD-1, CTLA-4, and PD-L2), indicating that the developed TTKPI may play an essential role in predicting the response to immunotherapy (Fig. 5a). Furthermore, we found that the expressions of the 8 genes (KIF11, SLC2A1, KCNMA1, BARHL2, CA9, TIMP1, MAGEC3, and PDZK1IP1) were significantly correlated with levels of immune checkpoint molecules, especially TIMP1 and KIF11 (Fig. 5b, c).

Furthermore, the TTKPI was tested for predicting the response to ICIs therapy in the IMvigor210 group (urothelial cancer, n=298), GSE91061 (melanoma, n=39) and GSE135222 (non-small cell lung cancer,

NSCLC, n=24). KM analysis indicated high-risk patients had poor OS following immunotherapy (Fig. 5d, g, i). The low-risk score was related to a positive response to anti-PD-L1 therapy (Fig. 5e and Supplementary Figs. 2a, b). The high-risk individuals also had a considerably worse clinical response to PD-L1 blocking medication than those with low-risk scores (14% vs. 31%, odds ratio [OR]: 2.66; 95% CI 1.50–4.99; $P < 0.001$, Fig. 5f). Similar trend was also identified in the validation cohort GSE91061 (11.1% vs. 54.5%, OR: 8.856856; 95% CI 1.366439, 75.086191; $P < 0.01$, Fig. 5h) as well as GSE135222 (7.7% vs. 45.5%, OR: 12.69929; 95% CI 1.118841–712.230160; $P < 0.05$, Fig. 5j). These results show that the low-risk individuals are more prone to benefit, and the TTKPI may serve as a valuable predictive biomarker for stratifying ESCC patients who may benefit from immunotherapy.

Identification of prognostic risk genes

To further determine the primary regulatory genes of TTK, we analyzed the correlations among 8 risk genes of TTKPI and observed significant synergistic effects (Fig. 6a). In the GSE53625 database, a general correlation was detected among these prognostic risk genes. Given our previous identification of KIF11 as the most potent prognostic factor (Fig. 2c), we subsequently concentrated our research on assessing the impact of KIF11 on ESCC prognosis. In survival analysis, the group with high KIF11 expression showed a poorer prognosis (Fig. 6b). Additionally, the differences in immune cell infiltration between high-risk and low-risk groups were explored using EPIC immune cell infiltration assessment methods from the TIMER 2.0 website [48]. In ESCC samples, KIF11 mRNA expression showed a negative correlation with CD8⁺ T cell infiltration (Fig. 6c). The purity index suggested that KIF11 expression increases with the proportion of tumor cells in tumor samples within the tumor microenvironment (TME) (Fig. 6c). This indicates that high KIF11 expression in tumor cells may suppress immune cell infiltration through specific mechanisms, thereby reducing the presence of non-tumor cells within the TME. To further investigate the relationship between KIF11 and CD8⁺ T cell infiltration in clinical samples, we performed mIHC staining on a tissue microarray from ESCC patients. The results showed that patients with high KIF11 expression had lower levels of CD8⁺ T cell infiltration (Fig. 6d). Taken together, these observations suggest that KIF11 is a key regulatory gene of TTK in ESCC, warranting further investigation. KIF11, a well-known kinesin superfamily member, is a protein-coding gene holding a critical position in various cancers, including breast, liver, gallbladder, and glioblastoma [49–52]. However, its involvement in ESCC has been relatively underreported. Thus, it emerged as the focal

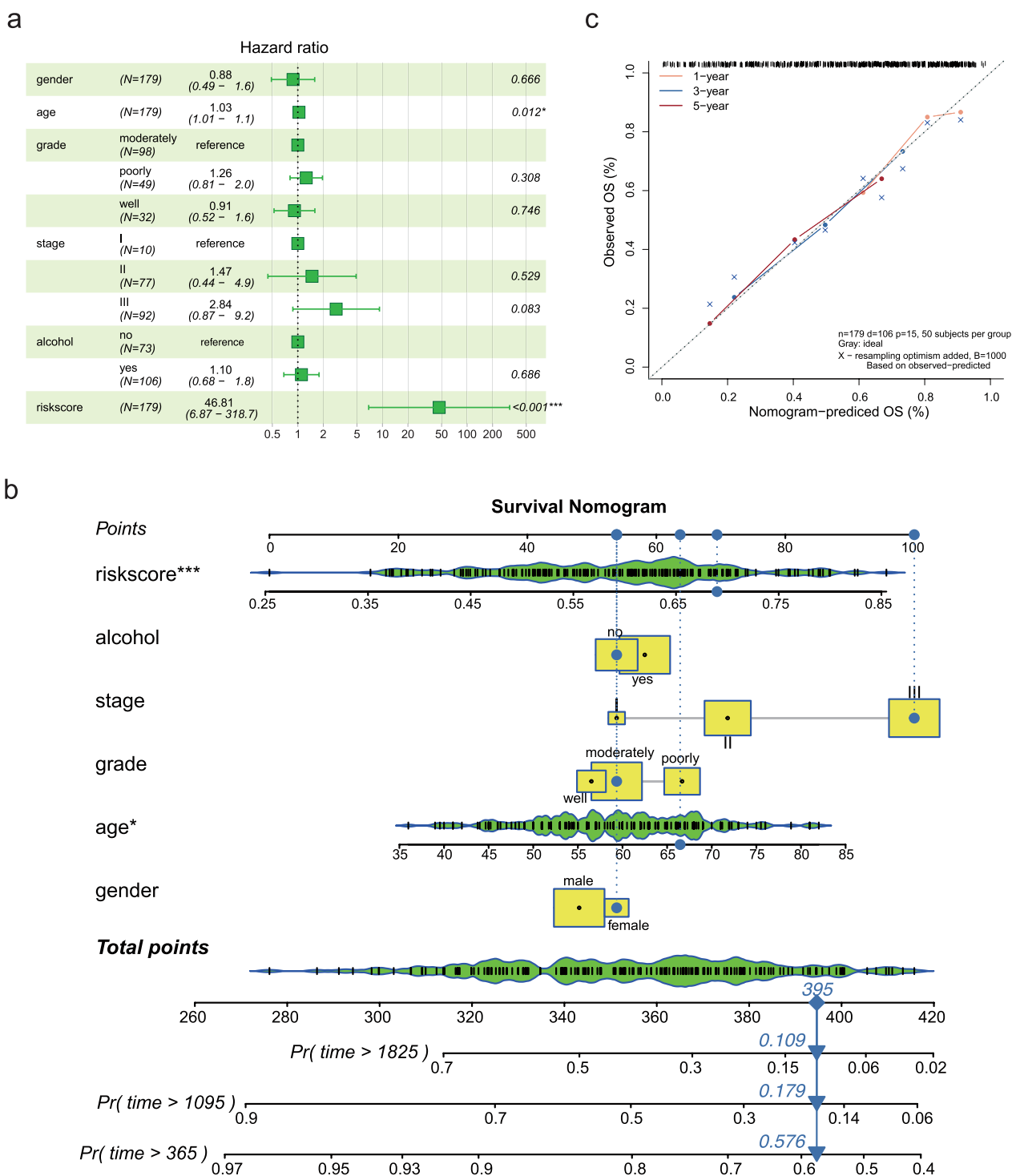


Fig. 4 Establishment and assessment of a TTKPI-based survival prediction nomogram. **a** Multivariate cox regression analysis of the clinical characteristics and TTKPI in the GSE53625 cohort. The green square indicates the HR value, and the error bars represent 95% confidence intervals. **b** A nomogram determining the prognostic of patients with ESCC. The blue plot shows a representative patient. **c** Calibration curves of the prognostic nomogram showing the consistency between the predicted and actually observed 1-, 3-, and 5-year OS. The 45-degree dashed line represents a perfect prediction, and the actual performances of our nomogram are shown by blue lines. Statistical analysis is performed with a Log-rank test (a). * $P < 0.05$, *** $P < 0.0001$

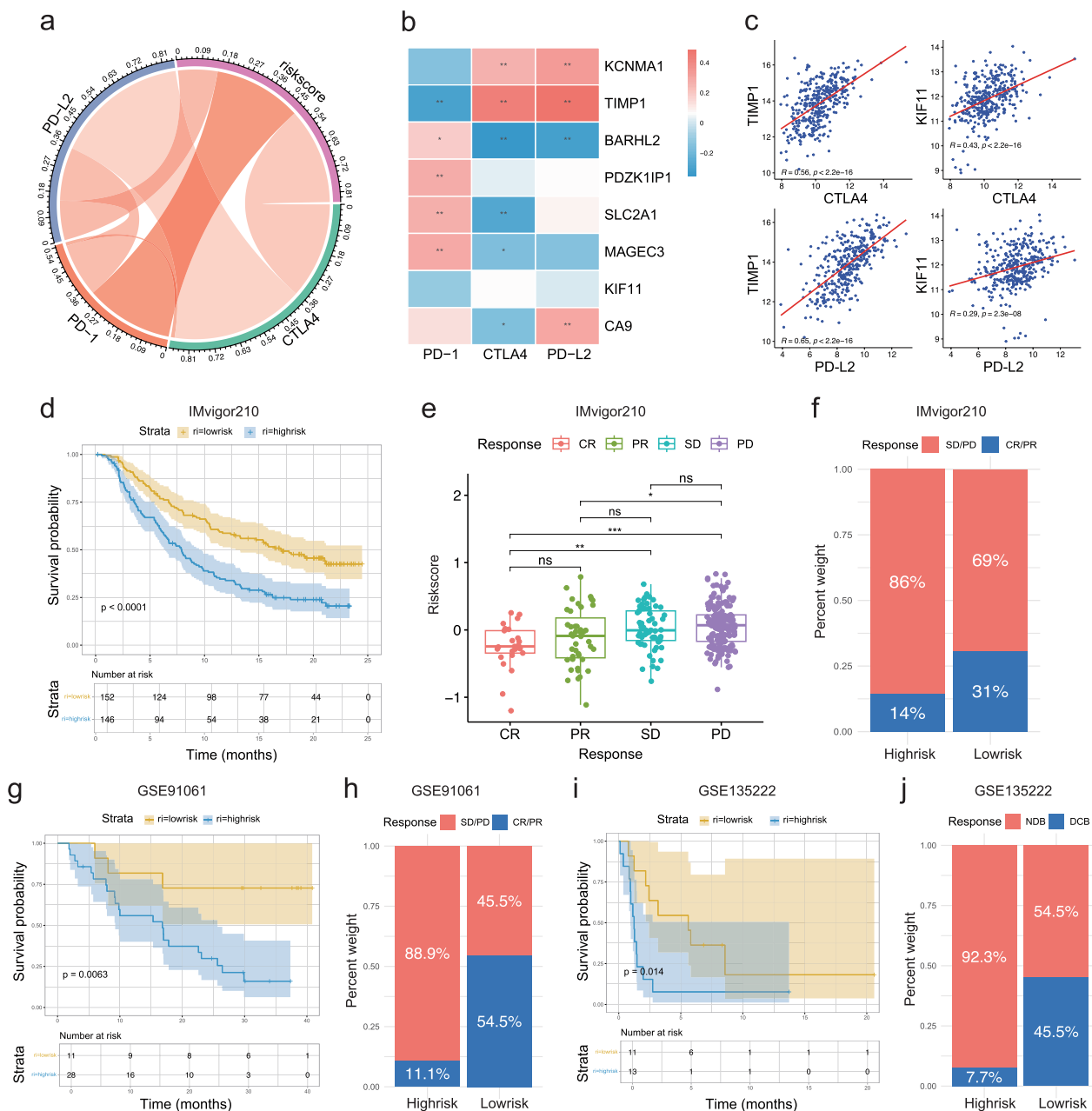


Fig. 5 Role of the TTKPI in predicting immunotherapeutic benefits. **a** Association between risk score signature and immune checkpoint molecules. **b** Association between the 8 genes and immune checkpoint molecules. **c** Correlation among TIMP1, KIF11, and CTLA4 expression. Correlation among TIMP1, KIF11, and PD-L2 expression. **d** KM survival curve in the IMvigor210 group (urothelial cancer, n = 298). **e** Risk scores in groups with different anti-PD-L1 clinical response status in the IMvigor210 group. **f** Proportion of patients with response to PD-L1 blockade therapy in the high-risk and low-risk score groups in the IMvigor210 group. **g** KM survival curve in the GSE91061 (melanoma, n = 39). **h** Proportion of patients with response to PD-L1 blockade therapy in the high-risk and low-risk score groups in the GSE91061. **i** KM survival curve in the GSE135222 (NSCLC, n = 24). **j** Proportion of patients with response to PD-L1 blockade therapy in the high-risk and low-risk score groups in the GSE135222. Statistical analysis is performed with Pearson correlation analysis (**a–c**), Log-rank test (**d, g, i**), Student’s t-test (**e**) and Fisher’s exact test (**f, h, i**). ns: no significance, ****** $P < 0.01$, ******* $P < 0.001$. CR: complete remission, PR: partial response, SD: stable disease, PD: progressive disease, DCB: durable clinical benefit, NDB: non-durable benefit

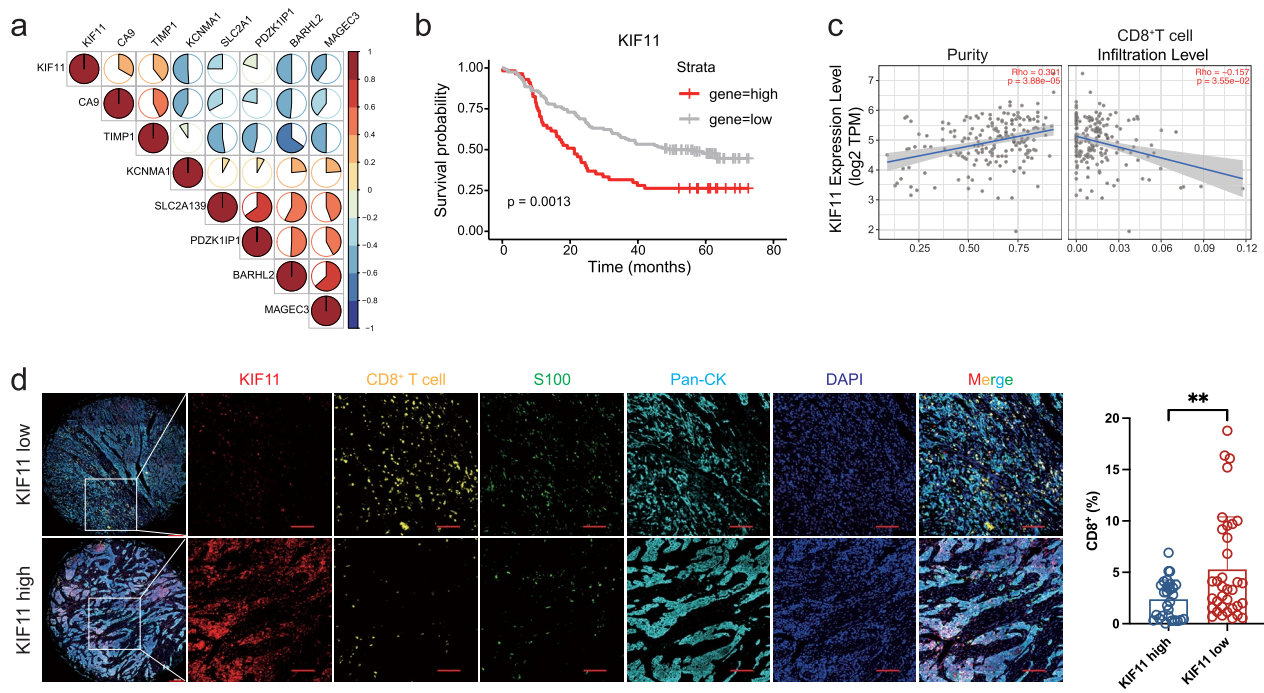


Fig. 6 Identification of prognostic risk genes. **a** Correlation analysis among the 8 best prognostic genes in GSE53625. **b** KM survival analysis displayed high the expression of KIF11 correlated with poor prognosis in ESCC patients. **c** The correlation of KIF11 mRNA expression with tumor cell purity (left) and the degree of CD8⁺ T cell infiltration (right) in ESCC was analyzed with TIMER 2.0. **d** mIHC stained by a ESCC tissue microarray. Representative pictures (left) of mIHC assay and the summarized results (right) are shown (n: 70 patients). The data are presented as the means \pm standard deviations (SD). Statistical analysis is performed with Pearson correlation analysis (**a**), Log-rank test (**b**), Wilcoxon test (**c**) and Student's t-test (**d**). * $P < 0.05$, ** $P < 0.01$, *** $P < 0.001$, **** $P < 0.0001$

point of this study aiming to capture a full and nuanced understanding.

KIF11 promotes cell proliferation and migration in vivo and in vitro

To confirm the significant role of KIF11 in ESCC, we measured the expression levels of KIF11 in six ESCC cell lines (Fig. 7a), and selected KYSE30 and KYSE450, which exhibited high expression level, for further study. Subsequently, we stably transfected two independent shRNAs targeting KIF11 in KYSE30 and KYSE450 (Figs. 7b, c). We observed a substantial decrease of cell viability upon KIF11 knockdown compared to the control group (Fig. 7d, e). Consistently, KIF11 inhibition led to a significantly decreased colony-forming rate in the colony formation assay (Fig. 7f, i). These results revealed the depletion of KIF11 significantly impaired ESCC cell proliferation. Additionally, a significant reduction of migration distance in wound-healing assay was observed in KIF11 knockdown group. A significant reduction in migration distance was observed following sh1 and sh2 transfections in ESCC cells, demonstrating a decreased metastatic potential upon KIF11 knockdown (Fig. 7g-j). To further investigate the effect of KIF11 on

tumor formation in vivo, KIF11-knockdown and control KYSE30 cells were subcutaneously injected into BALB/C nude mice. The results revealed that the tumor sizes and weights in KIF11 depletion group were markedly smaller than those in control group (Fig. 8a-c). In conclusion, our study suggests that KIF11 enhances the malignant proliferation and migration of ESCC cells both in vitro and in vivo.

Discussion

ICI therapy has been confirmed to be an effective strategy for patients with ESCC; however, the overall response rate to ICI in this patient population remains modest [10, 53–55]. Furthermore, there are no effective biomarkers for predicting immunotherapy response and OS in ESCC currently [15]. Thus, it is necessary to develop a signature to predict the survival of ESCC patients and increase the effectiveness of cancer immunotherapy. Immune infiltration and immunotherapy responses are closely linked, and immune cell failure increases the immunosuppressive state of malignancies [7]. However, the functions of T-cell activity have not yet received adequate attention, which may significantly impact the prognosis and treatment response, particularly in patients receiving

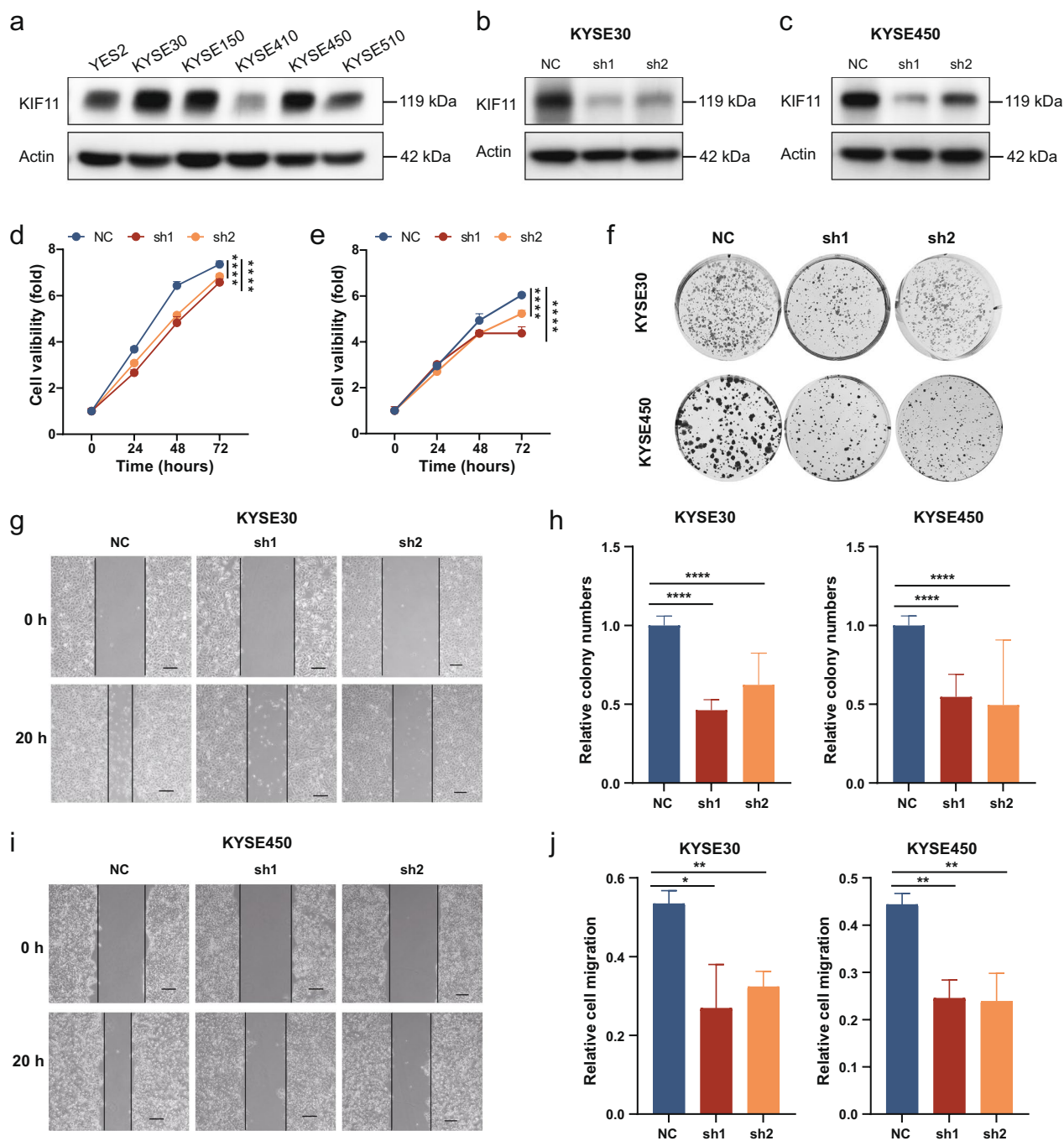


Fig. 7 KIF11 increases proliferation and migration of ESCC in vitro. **a** Western blot performed to assess KIF11 expression in YES2, KYSE30, KYSE150, KYSE410, KYSE450, and KYSE510 cells. **(b-c)** KIF11 levels in KYSE30 and KYSE450 cells transfected with shRNA (sh1, sh2) and control (NC) were analyzed using Western blot. **d-e** CCK-8 assays evaluating the proliferation capacity of KIF11-depleted KYSE30 and KYSE450 cells. **f** Colony formation assays to demonstrate changes in proliferation in KIF11-depleted KYSE30 and KYSE450 cells. **g** Statistical analysis of colony formation ability in KIF11-depleted KYSE30 and KYSE450 cells. **h, i** Representative micrographs showed the wound healing efficiency of KYSE30 and KYSE450 cells with reduced KIF11 expression using specific shRNA. **j** Statistical analysis of the scratch wound healing rate in KIF11-depleted KYSE30 and KYSE450 cells. The data are presented as the means \pm standard deviations (SD) of three independent experiments. Statistical analysis is performed with Student's t-test (**d, e, g, j**). * $P < 0.05$, ** $P < 0.01$, *** $P < 0.001$, **** $P < 0.0001$

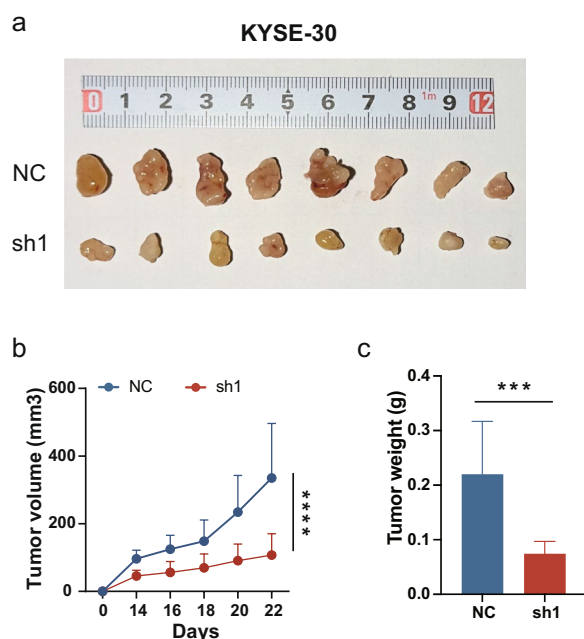


Fig. 8 KIF11 functions as a determinant regulating the growth and metastasis of ESCC cells in vivo. **a** KIF11-depleted KYSE30 and control KYSE30 cells were subcutaneously injected in BALB/C nude mice. After 4 weeks, the tumors were excised and photographed. **b** Tumor growth curves were plotted for the mice bearing KYSE30 cells. **c** Tumor weights were shown for the mice bearing KYSE30 cells. (n=8). The data are presented as the means \pm standard deviations (SD). Statistical analysis is performed with Student's t-test (**c**). *** $P < 0.001$, **** $P < 0.0001$

immunotherapy [7, 56, 57]. Furthermore, T-cell activity is linked to the prognosis of individuals with different solid malignancies [58]. Here, we developed a signature comprising 8 TTK-related genes that can predict the OS and disease-free survival of ESCC patients.

The GSE53625 cohort was used as the training dataset, and its excellent performance was validated in three external cohort (GSE53624, GSE47404 and TCGA-ESCC cohort). A nomogram comprising clinical features and TTKPI was developed; its performance was deemed satisfactory. Moreover, we observed that the TTKPI correlated with immunomodulators and immunotherapy. These results herald the possibility that the developed TTKPI is a reliable model for predicting survival and immunotherapeutic responses in ESCC, facilitating the development of novel ESCC treatment strategies.

Immunotherapy has provided new insights into ESCC treatment, with ICIs emerging as potentially viable treatments. Targeting immune checkpoint molecules has been identified as a potential approach to enhance antitumor immunity, such as PD-1 and

CTLA-4 [54]. Moreover, PD-1/PD-L1 inhibitors, such as pembrolizumab and nivolumab, have recently been approved for first-line treatment [53]. The correlation observed between the risk score signature and immune checkpoint molecules suggests that the TTKPI can potentially predict patient response to current anti-checkpoint immunotherapy. High-risk patients may have higher T-cell exclusion levels than low-risk patients, and their reduced response to ICI therapy may be attributed to immune evasion through T-cell exclusion [8]. The inferior OS observed in high-risk patients is potentially attributable to immune cell exhaustion, which has also been identified as the primary reason for low objective response rates to immunotherapy [59, 60].

To substantiate the predictive value of TTKPI further, we conducted a survival analysis of patients from the IMvigor210 cohort (urothelial cancer), GSE91061 (melanoma) and GSE135222 (NSCLC) who had received anti-PD-L1 therapy [44–47]. Our findings revealed that TTKPI effectively distinguished different outcomes among patients undergoing anti-PD-L1 therapy. Specifically, we found that patients classified as low-risk experienced significant therapeutic benefits more than high-risk patients, resulting in an improved clinical response. This underscores the potential of TTKPI as a valuable tool in identifying specific individuals who are more likely to own favorable responses to anti-PD-L1 therapy.

Understanding the TME may aid in developing novel ESCC treatments or increasing the efficacy of immunotherapy. TME immune status analysis has gained significant attention as a critical immunotherapy component [21, 61]. Moreover, among the 8 TTKPI genes, KIF11 was identified as a crucial prognostic indicator for ESCC patients, despite receiving limited attention in the ESCC so far. In this study, KIF11, as the most significant gene within the TTK signature, is significantly negatively correlated with CD8⁺ T cell infiltration, as observed in both EPIC immune cell infiltration analysis and mIHC staining. This suggests that KIF11 may serve as a marker of immune infiltration and could indicate the prognosis for immunotherapy of ESCC patients.

Our findings reveal that KIF11 plays a critical role in promoting ESCC malignancy by enhancing cell proliferation, migration, and tumor growth. Knockdown of KIF11 in KYSE30 and KYSE450 cell lines significantly reduced cell viability, colony formation, and migratory capacity, highlighting its importance in sustaining ESCC growth and metastatic potential. Consistently, in vivo experiments showed that KIF11 depletion markedly suppressed

tumor growth, further confirming its oncogenic role. These results suggest that KIF11 is a key driver of ESCC progression and may function as a valuable tumor biomarker facilitating the diagnosis and immune-related therapy of ESCC. Future studies should investigate the underlying mechanisms of KIF11's function and assess the potential of KIF11 inhibitors in preclinical and clinical settings to improve ESCC treatment outcomes.

Our study has considerable clinical applicability, and the developed TTKPI may be an effective and independent biomarker for forecasting the outcomes of ESCC patients. Furthermore, our findings may help in selecting patients for ICI therapy. Although our model exhibited excellent performance, it is crucial to recognize its limitations. Firstly, although the predictive risk score performed well, it still needs to be validated through large-scale prospective cohort studies. Additionally, while the use of dataset-specific cutoffs ensures statistical rigor within individual cohorts, the absence of a standardized global cutoff for TTKPI restricts its broader applicability and complicates cross-dataset validation. To address these limitations, future investigations should prioritize the development of consensus-driven global cutoff criteria and perform external validation of the TTKPI model across diverse datasets. Moreover, further *in vivo* studies on KIF11 are necessary, as the precise molecular mechanisms by which KIF11 influences ESCC progression remain unknown.

Conclusions

In summary, our integrative analysis established a useful survival predictor, TTKPI, which accurately predicts survival in ESCC, reflects the immunotherapy efficacy, and impacts clinical outcome evaluation. Importantly, we verified the characteristics and roles of the best predictive risk gene KIF11 of TTKPI, which could be a potential biomarker and therapeutic target in improving ESCC precision treatment.

Abbreviations

ESCC	Esophageal squamous cell carcinoma
ICI	Immune checkpoint inhibitor
PD-1	Programmed death 1
PD-L1	Programmed death-ligand 1
CTLA4	Cytotoxic T-lymphocyte-associated protein 4
TME	Tumor microenvironment
TTK	T cell-mediated tumor killing
TTKPI	TTK-related gene prognostic index
DEG	Differentially expressed gene
OS	Overall survival
KM	Kaplan–Meier
AUC	Area under the curve
CI	Confidence interval
OR	Odds ratio
HR	Hazard ratio
mIHC	Multiplex fluorescent immunohistochemistry

Supplementary Information

The online version contains supplementary material available at <https://doi.org/10.1186/s12967-025-06178-y>.

Supplementary Material 1. Fig. 1. Principal component analysis was carried out to assess the data quality and visualize the variability within the samples after batch-effect removal. The heatmap of DEGs between healthy and ESCC tissues demonstrated genetic differences between the two tissue types. KEGG analysis of 98 TTK-related DEGs. Univariate Cox regression analysis of the clinical characteristics and TTKPI in the GSE53625 cohort. Figure 2. Risk scores in groups with different anti-PD-L1 clinical response status in the GSE91061. Risk scores in groups with different anti-PD-L1 clinical response status in the GSE135222. Statistical analysis is performed with Student's t-test. ns: no significance, * $P < 0.05$, ** $P < 0.01$. CR: complete remission, PR: partial response, SD: stable disease, PD: progressive disease, DCB: durable clinical benefit, NDB: non-durable benefit. Table 1: The list of the TTK signature genes. Table 2: A detailed overview of the sample characteristics and clinical data for GSE53625.

Acknowledgements

We sincerely appreciate the contributions of TISIDB, TIMER2.0, GEO, and TCGA databases.

Author contributions

Q.M.Z. conceived and supervised the study. X.X.C. and H.H.Z. conducted the experiments. X.X.C., Q.N.W., H.H.Z., Z.W.L., L.P.Y., Q.J.M., and Q.M.Z. analyzed the results. X.X.C., Z.W.L., and Q.N.W. edited the manuscript. All the authors reviewed the manuscript.

Funding

This study was supported by the [National Natural Science Foundation of China #1] under Q. Zhan [number 81988101]; [National Key Research and Development Program of China #2] under Q. Wu [number 2021YFC2501001]; [Beijing Hospitals Authority Youth Programme #3] under Q. Wu, [number QML20231116].

Availability of data and materials

The datasets used during the current study are available and can be accessed through the following links: <http://www.ncbi.nlm.nih.gov/geo/> and <https://portal.gdc.cancer.gov/repositories>.

Declarations

Ethics approval and consent to participate

Not applicable.

Consent for publication

Not applicable.

Competing interests

The authors declare that they have no competing interests.

Author details

¹Key Laboratory of Carcinogenesis and Translational Research (Ministry of Education/Beijing), Laboratory of Molecular Oncology, Peking University Cancer Hospital & Institute, Beijing 100142, China. ²State Key Laboratory of Molecular Oncology, Beijing Key Laboratory of Carcinogenesis and Translational Research, Laboratory of Molecular Oncology, Peking University Cancer Hospital & Institute, Beijing 100142, China. ³Peking University International Cancer Institute, Beijing 100142, China. ⁴Department of Medical Oncology and Department of Talent Highland, The First Affiliated Hospital of Xi'an Jiaotong University, Xi'an 710061, China. ⁵Institute of Cytology and Genetics, Hengyang Medical College, University of South China, Hengyang 421001, Hunan, China.

Received: 20 August 2024 Accepted: 25 January 2025

Published online: 18 February 2025

References

- Bray F, Laversanne M, Sung H, Ferlay J, Siegel RL, Soerjomataram I, Jemal A. Global cancer statistics 2022: GLOBOCAN estimates of incidence and mortality worldwide for 36 cancers in 185 countries. *CA Cancer J Clin*. 2024;74:229–63.
- Chen W, Zheng R, Baade PD, Zhang S, Zeng H, Bray F, Jemal A, Yu XQ, He J. Cancer statistics in China, 2015. *CA Cancer J Clin*. 2016;66:115–32.
- Zeng H, Chen W, Zheng R, Zhang S, Ji JS, Zou X, Xia C, Sun K, Yang Z, Li H. Changing cancer survival in China during 2003–15: a pooled analysis of 17 population-based cancer registries. *Lancet Glob Health*. 2018;6:e555–67.
- Song Y, Li L, Ou Y, Gao Z, Li E, Li X, Zhang W, Wang J, Xu L, Zhou Y, et al. Identification of genomic alterations in oesophageal squamous cell cancer. *Nature*. 2014;509:91–5.
- Wu H-X, Pan Y-Q, He Y, Wang Z-X, Guan W-L, Chen Y-X, Yao Y-C, Shao N-Y, Xu R-H, Wang F. Clinical benefit of first-line programmed death-1 antibody plus chemotherapy in low programmed cell death ligand 1-expressing esophageal squamous cell carcinoma: a post hoc analysis of JUPITER-06 and meta-analysis. *J Clin Oncol*. 2023;41:1735–46.
- Waldman AD, Fritz JM, Lenardo MJ. A guide to cancer immunotherapy: from T cell basic science to clinical practice. *Nat Rev Immunol*. 2020;20:651–68.
- O'Donnell JS, Teng MW, Smyth MJ. Cancer immunoeediting and resistance to T cell-based immunotherapy. *Nat Rev Clin Oncol*. 2019;16:151–67.
- Jiang P, Gu S, Pan D, Fu J, Sahu A, Hu X, Li Z, Traugh N, Bu X, Li B. Signatures of T cell dysfunction and exclusion predict cancer immunotherapy response. *Nat Med*. 2018;24:1550–8.
- Philip M, Schietinger A. CD8(+) T cell differentiation and dysfunction in cancer. *Nat Rev Immunol*. 2022;22:209–23.
- Chen G, Huang AC, Zhang W, Zhang G, Wu M, Xu W, Yu Z, Yang J, Wang B, Sun H, et al. Exosomal PD-L1 contributes to immunosuppression and is associated with anti-PD-1 response. *Nature*. 2018;560:382–6.
- Kojima T, Shah MA, Muro K, Francois E, Adenis A, Hsu C-H, Doi T, Moriwaki T, Kim S-B, Lee S-H. Randomized phase III KEYNOTE-181 study of pembrolizumab versus chemotherapy in advanced esophageal cancer. *J Clin Oncol*. 2020;38:4138–48.
- Weber JS, D'Angelo SP, Minor D, Hodi FS, Gutzmer R, Neyns B, Hoeller C, Khushalani NI, Miller WH, Lao CD. Nivolumab versus chemotherapy in patients with advanced melanoma who progressed after anti-CTLA-4 treatment (CheckMate 037): a randomised, controlled, open-label, phase 3 trial. *Lancet Oncol*. 2015;16:375–84.
- Network CGAR. Integrated genomic characterization of oesophageal carcinoma. *Nature*. 2017;541:169.
- Vasan N, Baselga J, Hyman DM. A view on drug resistance in cancer. *Nature*. 2019;575:299–309.
- Hegde PS, Chen DS. Top 10 challenges in cancer immunotherapy. *Immunity*. 2020;52:17–35.
- Galassi C, Chan TA, Vitale I, Galluzzi L. The hallmarks of cancer immune evasion. *Cancer Cell*. 2024. <https://doi.org/10.1016/j.ccell.2024.09.010>.
- Leone RD, Powell JD. Metabolism of immune cells in cancer. *Nat Rev Cancer*. 2020;20:516–31.
- Cristescu R, Mogg R, Ayers M, Albricht A, Murphy E, Yearley J, Sher X, Liu XQ, Lu H, Nebozhyn M. Pan-tumor genomic biomarkers for PD-1 checkpoint blockade-based immunotherapy. *Science*. 2018;362:eaar3593.
- Cui Y, Chen H, Xi R, Cui H, Zhao Y, Xu E, Yan T, Lu X, Huang F, Kong P. Whole-genome sequencing of 508 patients identifies key molecular features associated with poor prognosis in esophageal squamous cell carcinoma. *Cell Res*. 2020;30:902–13.
- Zhang X, Gari A, Li M, Chen J, Qu C, Zhang L, Chen J. Combining serum inflammation indexes at baseline and post treatment could predict pathological efficacy to anti-PD-1 combined with neoadjuvant chemotherapy in esophageal squamous cell carcinoma. *J Transl Med*. 2022;20:61.
- Zheng Y, Chen Z, Han Y, Han L, Zou X, Zhou B, Hu R, Hao J, Bai S, Xiao H, et al. Immune suppressive landscape in the human esophageal squamous cell carcinoma microenvironment. *Nat Commun*. 2020;11:6268.
- Li Y, Lu Z, Che Y, Wang J, Sun S, Huang J, Mao S, Lei Y, Chen Z, He J. Immune signature profiling identified predictive and prognostic factors for esophageal squamous cell carcinoma. *Oncoimmunology*. 2017;6:e1356147.
- Pan D, Kobayashi A, Jiang P, Ferrari de Andrade L, Tay RE, Luoma AM, Tsoucas D, Qiu X, Lim K, Rao P, et al. A major chromatin regulator determines resistance of tumor cells to T cell-mediated killing. *Science*. 2018;359:770–775.
- Ru B, Wong CN, Tong Y, Zhong JY, Zhong SSW, Wu WC, Chu KC, Wong CY, Lau CY, Chen I. TISIDB: an integrated repository portal for tumor-immune system interactions. *Bioinformatics*. 2019;35:4200–2.
- Hirokawa N, Noda Y, Tanaka Y, Niwa S. Kinesin superfamily motor proteins and intracellular transport. *Nat Rev Mol Cell Biol*. 2009;10:682–96.
- Camlin NJ, McLaughlin EA, Holt JE. Motoring through: the role of kinesin superfamily proteins in female meiosis. *Hum Reprod Update*. 2017;23:409–20.
- Mann BJ, Wadsworth P. Kinesin-5 regulation and function in mitosis. *Trends Cell Biol*. 2019;29:66–79.
- Gao W, Lu J, Yang Z, Li E, Cao Y, Xie L. Mitotic functions and characters of KIF11 in cancers. *Biomolecules*. 2024;14:386.
- Kapitein LC, Peterman EJ, Kwok BH, Kim JH, Kapoor TM, Schmidt CF. The bipolar mitotic kinesin Eg5 moves on both microtubules that it crosslinks. *Nature*. 2005;435:114–8.
- Venere M, Horbinski C, Crish JF, Jin X, Vasani A, Major J, Burrows AC, Chang C, Prokop J, Wu Q. The mitotic kinesin KIF11 is a driver of invasion, proliferation, and self-renewal in glioblastoma. *Sci Transl Med*. 2015;7:304ra143–304ra143.
- Wei D, Rui B, Qingquan F, Chen C, Ping HY, Xiaoling S, Hao W, Jun G. KIF11 promotes cell proliferation via ERBB2/PI3K/AKT signaling pathway in gallbladder cancer. *Int J Biol Sci*. 2021;17:514–26.
- Shi S, Guo D, Ye L, Li T, Fei Q, Lin M, Yu X, Jin K, Wu W. Knockdown of TACC3 inhibits tumor cell proliferation and increases chemosensitivity in pancreatic cancer. *Cell Death Dis*. 2023;14:778.
- Sawada G, Niida A, Hirata H, Komatsu H, Uchi R, Shimamura T, Takahashi Y, Kurashige J, Matsumura T, Ueo H. An integrative analysis to identify driver genes in esophageal squamous cell carcinoma. *PLoS ONE*. 2015;10: e0139808.
- Li J, Chen Z, Tian L, Zhou C, He MY, Gao Y, Wang S, Zhou F, Shi S, Feng X. LncRNA profile study reveals a three-lncRNA signature associated with the survival of patients with oesophageal squamous cell carcinoma. *Gut*. 2014;63:1700–10.
- Ritchie ME, Phipson B, Wu D, Hu Y, Law CW, Shi W, Smyth GK. Limma powers differential expression analyses for RNA-sequencing and microarray studies. *Nucleic Acids Res*. 2015;43:e47–e47.
- Villanueva RAM, Chen ZJ: ggplot2: elegant graphics for data analysis. Taylor & Francis; 2019.
- Yu G, Wang L-G, Han Y, He Q-Y. clusterProfiler: an R package for comparing biological themes among gene clusters. *OMICS*. 2012;16:284–7.
- Tibshirani R. The lasso method for variable selection in the Cox model. *Stat Med*. 1997;16:385–95.
- Friedman JH, Hastie T, Tibshirani R. Regularization paths for generalized linear models via coordinate descent. *J Stat Softw*. 2010;33:1–22.
- Hothorn T: maxstat: Maximally Selected Rank Statistics. R package version 0.7–25. R Project; 2017.
- Kassambara A, Kosinski M, Biecek P: survminer: Drawing Survival Curves using ggplot2. CRAN: Contributed Packages 2016.
- Therneau T: A package for survival analysis in S. version 2.38. 2015.
- Harrell FE Jr. rms: Regression modeling strategies. R Pack Vers. 2016;5:1–263.
- Mariathasan S, Turley SJ, Nickles D, Castiglioni A, Yuen K, Wang Y, Kadel III EE, Koeppen H, Astarita JL, Cubas R. TGFβ attenuates tumour response to PD-L1 blockade by contributing to exclusion of T cells. *Nature*. 2018;554:544–8.
- Riaz N, Havel JJ, Makarov V, Desrichard A, Urba WJ, Sims JS, Hodi FS, Martin-Algarra S, Mandal R, Sharfman WH. Tumor and microenvironment evolution during immunotherapy with nivolumab. *Cell*. 2017;171(934–949): e916.
- Jung H, Kim HS, Kim JY, Sun J-M, Ahn JS, Ahn M-J, Park K, Esteller M, Lee S-H, Choi JK. DNA methylation loss promotes immune evasion of tumours with high mutation and copy number load. *Nat Commun*. 2019;10:4278.
- Balar AV, Galsky MD, Rosenberg JE, Powles T, Petrylak DP, Bellmunt J, Loriot Y, Necchi A, Hoffman-Censits J, Perez-Gracia JL. Atezolizumab as first-line treatment in cisplatin-ineligible patients with locally advanced and metastatic urothelial carcinoma: a single-arm, multicentre, phase 2 trial. *Lancet*. 2017;389:67–76.

48. Racle J, de Jonge K, Baumgaertner P, Speiser DE, Gfeller D. Simultaneous enumeration of cancer and immune cell types from bulk tumor gene expression data. *Elife*. 2017;6:e26476.
49. Wei D, Rui B, Qingquan F, Chen C, Xiaoling S, Hao W, Jun G. KIF11 promotes cell proliferation via ERBB2/PI3K/AKT signaling pathway in gallbladder cancer. *Int J Biol Sci*. 2021;17:514.
50. Zhou J, Chen W-R, Yang L-C, Wang J, Sun J-Y, Zhang W-W, He Z-Y, Wu S-G. KIF11 functions as an oncogene and is associated with poor outcomes from breast cancer. *Cancer Res Treat*. 2019;51:1207–21.
51. Jiang M, Zhuang H, Xia R, Gan L, Wu Y, Ma J, Sun Y, Zhuang Z. KIF11 is required for proliferation and self-renewal of docetaxel resistant triple negative breast cancer cells. *Oncotarget*. 2017;8:92106.
52. Venere M, Horbinski C, Crish JF, Jin X, Vasarji A, Major J, Burrows AC, Chang C, Prokop J, Wu Q: The mitotic kinesin KIF11 is a driver of invasion, proliferation, and self-renewal in glioblastoma. *Sci Transl Med* 2015, 7:304ra143–304ra143.
53. Sun J-M, Shen L, Shah MA, Enzinger P, Adenis A, Doi T, Kojima T, Metges J-P, Li Z, Kim S-B. Pembrolizumab plus chemotherapy versus chemotherapy alone for first-line treatment of advanced oesophageal cancer (KEYNOTE-590): a randomised, placebo-controlled, phase 3 study. *Lancet*. 2021;398:759–71.
54. Creelan BC, Wang C, Teer JK, Toloza EM, Yao J, Kim S, Landin AM, Mullinax JE, Saller JJ, Saltos AN. Tumor-infiltrating lymphocyte treatment for anti-PD-1-resistant metastatic lung cancer: a phase 1 trial. *Nat Med*. 2021;27:1410–8.
55. Meng X, Wu T, Hong Y, Fan Q, Ren Z, Guo Y, Yang X, Shi P, Yang J, Yin X, et al. Camrelizumab plus apatinib as second-line treatment for advanced oesophageal squamous cell carcinoma (CAP 02): a single-arm, open-label, phase 2 trial. *Lancet Gastroenterol Hepatol*. 2022;7:245–53.
56. Chou C, Zhang X, Krishna C, Nixon BG, Dadi S, Capistrano KJ, Kansler ER, Steele M, Han J, Shyu A, et al. Programme of self-reactive innate-like T cell-mediated cancer immunity. *Nature*. 2022;605:139–45.
57. Byrne A, Savas P, Sant S, Li R, Virassamy B, Luen SJ, Beavis PA, Mackay LK, Neeson PJ, Loi S. Tissue-resident memory T cells in breast cancer control and immunotherapy responses. *Nat Rev Clin Oncol*. 2020;17:341–8.
58. van der Leun AM, Thommen DS, Schumacher TN. CD8(+) T cell states in human cancer: insights from single-cell analysis. *Nat Rev Cancer*. 2020;20:218–32.
59. Baessler A, Vignali DA. T cell exhaustion. *Ann Rev Immunol*. 2024. <https://doi.org/10.1146/annurev-immunol-090222-110914>.
60. Chow A, Perica K, Klebanoff CA, Wolchok JD. Clinical implications of T cell exhaustion for cancer immunotherapy. *Nat Rev Clin Oncol*. 2022;19:775–90.
61. Binnewies M, Roberts EW, Kersten K, Chan V, Fearon DF, Merad M, Coussens LM, Gabrilovich DI, Ostrand-Rosenberg S, Hedrick CC, et al. Understanding the tumor immune microenvironment (TIME) for effective therapy. *Nat Med*. 2018;24:541–50.

Publisher's Note

Springer Nature remains neutral with regard to jurisdictional claims in published maps and institutional affiliations.